Faraday Discuss. Chem. Soc., 1987, **84**, 371-385

$\mathscr{L}^2$ Calculations of Accurate Quantal-dynamical Reactive Scattering Transition Probabilities and their Use to test Semiclassical Applications

John Z. H. Zhang, Yici Zhang and Donald J. Kouri
Departments of Chemistry and Physics, University of Houston, Houston, Texas 77004, U.S.A.

Bruce C. Garrett
Chemical Dynamics Corporation, 9530 Pennsylvania Avenue, Upper Marlboro, Maryland 20772, U.S.A.

Kenneth Haug, David W. Schwenke and Donald G. Truhlar*
Department of Chemistry and Supercomputer Institute, University of Minnesota, Minneapolis, Minnesota 55455, U.S.A.

We discuss the calculation of quantum-mechanical amplitudes for reactive scattering based on the Fock scheme for coupling arrangement channels and expansion of the coupled amplitude densities in terms of square-integrable ($\mathscr{L}^2$) basis functions. First, we provide a derivation of the coupled equations for the amplitude densities from the Fock-scheme integrodifferential equations for wavefunction components. Then we discuss the solution of these equations by $\mathscr{L}^2$ techniques. The methods are applied to calculate the thresholds and tunnelling probabilities for the reactions $O + H_2(v = 0, 1) \rightarrow OH + H$ and $H + OH(v = 0, 1) \rightarrow O + H_2$, where v denotes the vibrational quantum number. The results, which represent accurate quantal dynamics for a given potential-energy surface, are used to test the predictions of variational transition-state theory for threshold energies and the least-action semiclassical method for tunnelling probabilities.

1. Introduction

The calculation of quantum-mechanical transition amplitudes for reactive collision processes is a subject of great fundamental interest,[1] but progress has been slow owing to the difficulty of formulating the general problem in a way that is both numerically convenient and rapidly convergent. From the point of view of modern molecular quantum mechanics, the solution of the problem by a variational expansion in a square-integrable basis defined in coordinates related linearly to Cartesians has many advantages. These include ease of integral evaluation, vectorization[2] and the eventual possibility of using highly optimized basis sets. The simplest way to build basis sets that efficiently span the critical intermediate-coupling regions for reactive collisions is to use separate, non-orthogonal sets of direct product bases representing each reactant and product's translational, vibrational and rotational degrees of freedom. In principle, linear combinations of two or more such bases could be overcomplete,[3] but there are several possible ways to couple the various reactant and product arrangements that converge to unique, well defined answers.[4] We,[5,6] as well as Kuruoglu and Levin,[7,8] have found that one of these, the Fock coupling scheme, leads to particularly fast convergence. We have proposed therefore that the equations of the Fock coupling scheme be solved by $\mathscr{L}^2$ expansion of the wavefunction or amplitude-density components

corresponding to the various arrangements, and we have had good success with this approach.[5,6,9,10] In the present article we present another derivation of the Fock scheme coupled equations plus some results for the reaction $O+H_2 \leftrightarrow OH+H$ in section 3.

One of the primary motivations for obtaining converged quantal transition probabilities for prototype systems is to use them as benchmarks against which to test more approximate dynamical techniques. This is carried out in the present paper by using the accurate results to test variational transition state theory predictions of reaction thresholds and least-action semiclassical calculations of tunnelling probabilities.

In keeping with the goal of treating the quantal dynamics accurately for a prototype system, the present study treats $O+H_2$ as an electronically adiabatic reaction of distinguishable particles governed by a single potential-energy surface given by a convenient (though realistic) analytic function.

2. Derivation of Coupled Integrodifferential Equations for the Amplitude Density Components

In ref. (6) we presented a derivation of the coupled integral equations for reactive-scattering arrangement components of the amplitude density by starting with the Lippmann-Schwinger integral equation for the wavefunction. In this section we provide an alternate derivation of our amplitude density integral equations by starting with the Fock-type integrodifferential equations for translational wavefunctions commonly used in treatments of electron-atom or electron-molecule scattering.[11,12] This same approach has also been used by Miller[13] for atom-diatom reactive scattering. The integrodifferential equations may be derived by the application of the Kohn variational principle to a coupled-channel trial wavefunction for the Schrödinger equation.[11,14] In some cases, intrinsically $\mathscr{L}^2$-type functions have also been included in the trial wavefunction,[12-17] but we shall not include them in our discussion. In fact we shall introduce $\mathscr{L}^2$ functions only later, in section 3, by expanding the translational coordinate dependences of the amplitude densities.

We use the same notation as in ref. (6). In particular, the arrangements are labelled by α, where $\alpha = 1$, 2 or 3 denotes A+BC, B+AC and C+AB, respectively. We scale all coordinates to a reduced mass of

$$\mu = \left(\frac{m_A m_B m_C}{m_A + m_B + m_C} \right)^{1/2} \tag{1}$$

and we denote the mass-scaled Jacobi coordinate in arrangement α by $\boldsymbol{r}_\alpha$ for the diatom and $\boldsymbol{R}_\alpha$ for relative motion of the atom and the diatom.

Each channel is labelled by α and a collective quantum number $n = \{v_n, j_n, l_n\}$, where v_n is a vibrational quantum number associated with r_α, j_n is a rotational quantum number associated with $\hat{\boldsymbol{r}}_\alpha$ and l_n is an orbital quantum number associated with $\hat{\boldsymbol{R}}_\alpha$. The wavefunction, $\Psi^{\alpha_i n_i}$, is labelled by the initial values α_i and n_i of α and n, and it is expanded as

$$\Psi^{\alpha_i n_i} = \sum_{\alpha=1}^{3} \sum_{n=\bar{n}_\alpha}^{\bar{\bar{n}}_\alpha} R_\alpha^{-1} \phi_{\alpha n}(\boldsymbol{r}_\alpha, \hat{\boldsymbol{R}}_\alpha) F_{\alpha n}^{\alpha_i n_i}(R_\alpha) \tag{2}$$

where $\bar{n}_\alpha = \{1, N_1+1, N_1+N_2+1\}$, $\bar{\bar{n}}_\alpha = \{N_1, N_1+N_2, N_c\}$, $\phi_{\alpha n}$ is a channel basis function and $F_{\alpha n}^{\alpha_i n_i}$ is a translational radial wavefunction. Note that each channel has a unique n, so the arrangement index is merely informational, and it need not be specified as an index for summations or for components of vectors and matrices.

In each arrangement we partition the Hamiltonian as

$$H = H_\alpha^A + V_\alpha^D + V_\alpha^C \tag{3}$$

where

$$H_\alpha^{\mathrm{A}} = \lim_{R_\alpha \to \infty} H \tag{4}$$

and

$$V_\alpha^{\mathrm{D}} = \sum_{n=\bar{n}_\alpha}^{\bar{\bar{n}}_\alpha} |\phi_{\alpha n}\rangle V_{\alpha n}^{\mathrm{D}} \langle \phi_{\alpha n}|. \tag{5}$$

Note that H_α^{A} is the asymptotic Hamiltonian, including all the kinetic-energy terms, V_α^{D} is the distortion potential, $V_{\alpha n}^{\mathrm{D}}$ is a single-channel distortion potential defined for convenience and to accelerate convergence, and V_α^{C} is a coupling potential without which all rearrangement scattering amplitudes would be zero. The channel wavenumber $k_{\alpha vj}$ is defined by

$$k_{\alpha vj}^2 = (2\mu/\hbar^2)(E - \varepsilon_{\alpha vj}) \tag{6}$$

where

$$H_\alpha^{\mathrm{A}} \phi_{\alpha n}(\boldsymbol{r}_\alpha, \hat{R}_\alpha) = \left(\varepsilon_{\alpha v_n j_n} + \frac{\hbar l_n(l_n+1)}{2\mu R_\alpha^2} \right) \phi_{\alpha n}(\boldsymbol{r}_\alpha, \hat{R}_\alpha). \tag{7}$$

With this partitioning of the Hamiltonian, the integrodifferential equations of ref. (13) may be written as

$$\left(\frac{\mathrm{d}^2}{\mathrm{d}R_\alpha^2} - \frac{2\mu}{\hbar^2} V_{\alpha n}^{\mathrm{D}} - \frac{l_n(l_n+1)}{R_\alpha^2} + k_{\alpha v_n j_n}^2 \right) F_{\alpha n}^{\alpha_0 n_0}(R_\alpha) = \frac{2\mu}{\hbar^2} \sum_{n'} (\mathcal{T}_{\alpha n \alpha' n'} + \mathcal{V}_{\alpha n \alpha' n'}) F_{\alpha' n'}^{\alpha_0 n_0}, \tag{8}$$

where the (in general non-local) operators $\mathcal{T}_{\alpha n \alpha' n'}$ and $\mathcal{V}_{\alpha n \alpha' n'}$ are given by

$$\begin{aligned} \mathcal{T}_{\alpha n \alpha' n'} F_{\alpha' n'}^{\alpha_0 n_0} = (\delta_{\alpha\alpha'} - 1) R_\alpha \int \mathrm{d}\hat{R}_\alpha \, \mathrm{d}\boldsymbol{r}_\alpha \phi_{\alpha n}^*(\boldsymbol{r}_\alpha, \hat{R}_\alpha) \\ \times [R_{\alpha'}(\boldsymbol{R}_\alpha, \boldsymbol{r}_\alpha)]^{-1} \phi_{\alpha' n'}[\boldsymbol{r}_{\alpha'}(\boldsymbol{R}_\alpha, \boldsymbol{r}_\alpha), \hat{R}_{\alpha'}, (\boldsymbol{R}_\alpha, \boldsymbol{r}_\alpha)] \\ \times \frac{\hbar^2}{2\mu} \left(\frac{\mathrm{d}^2}{\mathrm{d}R_{\alpha'}^2} - \frac{l_{n'}(l_{n'}+1)}{R_{\alpha'}^2} - \frac{2\mu}{\hbar^2} V_{\alpha' n'}^D + k_{\alpha' v_{n'} j_{n'}}^2 \right) F_{\alpha' n'}^{\alpha_0 n_0}[R_{\alpha'}(\boldsymbol{R}_\alpha, \boldsymbol{r}_\alpha)] \end{aligned} \tag{9}$$

and

$$\begin{aligned} \mathcal{V}_{\alpha n \alpha' n'} F_{\alpha' n'}^{\alpha_0 n_0} = R_\alpha \int \mathrm{d}\hat{R}_\alpha \, \mathrm{d}\boldsymbol{r}_\alpha \phi_{\alpha n}^*(\boldsymbol{r}_\alpha, \hat{R}_\alpha) V_{\alpha'}^{\mathrm{C}}[\boldsymbol{R}_{\alpha'}(\boldsymbol{R}_\alpha, \boldsymbol{r}_\alpha), \boldsymbol{r}_{\alpha'}(\boldsymbol{R}_\alpha, \boldsymbol{r}_\alpha)] \\ \times \phi_{\alpha' n'}[\boldsymbol{r}_{\alpha'}(\boldsymbol{R}_\alpha, \boldsymbol{r}_a), \hat{R}_{\alpha'}(\boldsymbol{R}_\alpha, \boldsymbol{r}_\alpha)][R_{\alpha'}(\boldsymbol{R}_\alpha, \boldsymbol{r}_\alpha)]^{-1} F_{\alpha' n'}^{\alpha_0 n_0}[R_{\alpha'}(\boldsymbol{R}_\alpha, \boldsymbol{r}_\alpha)]. \end{aligned} \tag{10}$$

It is useful to define a distorted-wave radial Green's function as the solution of

$$\left(\frac{\mathrm{d}^2}{\mathrm{d}R_\alpha^2} - \frac{l_n(l_n+1)}{R_\alpha^2} - \frac{2\mu V_{\alpha n}^{\mathrm{D}}(R_\alpha)}{\hbar^2} + k_{\alpha v_n j_n}^2 \right) g_n^\alpha(R_\alpha, R'_\alpha) = \frac{2\mu}{\hbar^2} \delta(R_\alpha - R'_\alpha). \tag{11}$$

Then, if ${}^{(r)}f_n^\alpha$ and ${}^{(i)}f_n^\alpha$ are, respectively, the regular and irregular solutions of the homogeneous analogue of eqn (11), the standard solution for the Green's function is

$$g_n^\alpha(R_\alpha, R'_\alpha) = -\frac{2\mu}{\hbar^2} {}^{(i)}f_n^\alpha(R_\alpha^>) {}^{(r)}f_n^\alpha(R_\alpha^<) \tag{12}$$

where $R_\alpha^<(R_\alpha^>)$ is the lesser (greater) of R_α, R'_α. Note that for open channels

$${}^{(\mathrm{r})}f_n^\alpha \underset{R_\alpha \to \infty}{\sim} k_{\alpha v_n j_n}^{1/2} R_\alpha [j_{l_n}(k_{\alpha v_n j_n} R_\alpha) - {}^0K_n^\alpha n_{l_n}(k_{\alpha v_n j_n} R_\alpha)] \tag{13a}$$

$${}^{(\mathrm{i})}f_n^\alpha \underset{R_\alpha \to 0}{\sim} k_{\alpha v_n j_n}^{1/2} n_{l_n}(k_{\alpha v_n j_n} R_\alpha) \tag{13b}$$

where j_l and n_l are spherical Bessel and Neumann functions and where ${}^0K_n^\alpha$ is the tangent of the distorted-wave phase shift. Then the formal solution of eqn (8) is

$$F_{\alpha n}^{\alpha_0 n_0}(R_\alpha) = \delta_{\alpha\alpha_0}\delta_{nn_0} {}^{(\mathrm{r})}f_n^\alpha(R_\alpha) - \frac{2\mu}{\hbar^2} \int_0^\infty \mathrm{d}R'_\alpha \, {}^{(\mathrm{i})}f_n^\alpha(R_\alpha^>) {}^{(\mathrm{r})}f_n^\alpha(R_\alpha^<) \sum_{n'} (\mathcal{T}_{\alpha n \alpha' n'} + \mathcal{V}_{\alpha n \alpha' n'}) F_{\alpha' n'}^{\alpha_0 n_0}. \tag{14}$$

We then introduce the radial amplitude density, defined as

$$\zeta_{\alpha n}^{\alpha_0 n_0}(R_\alpha) = \sum_{n'} (\mathscr{T}_{\alpha n \alpha' n'} + \mathscr{V}_{\alpha n \alpha' n'}) F_{\alpha' n'}^{\alpha_0 n_0} \tag{15}$$

so that the reactance matrix may be written

$$K_{n_f n_i} = \delta_{n_f n_i}{}^0 K_{n_i}^{\alpha_i} + \mathscr{K}_{n_f n_i} \tag{16}$$

where

$$\mathscr{K}_{n_f n_i} = -\frac{2\mu}{\hbar^2} \int_0^\infty \mathrm{d}R_{\alpha_f}\, {}^{(\mathrm{r})}f_{n_f}^{\alpha}(R_{\alpha_f}) \zeta_{\alpha_f n_f}^{\alpha_i n_i}(R_{\alpha_f}). \tag{17}$$

To obtain a closed set of coupled equations for the $\zeta_{\alpha' n'}^{\alpha_0 n_0}$, we substitute eqn (15) into (14), apply $(\mathscr{T}_{\alpha' n' \alpha n} + \mathscr{V}_{\alpha' n' \alpha n})$, and sum over n to yield

$$\begin{aligned}\zeta_{\alpha' n'}^{\alpha_0 n_0}(R_{\alpha'}) = {} & (\mathscr{T}_{\alpha' n' \alpha_0 n_0} + \mathscr{V}_{\alpha' n' \alpha_0 n_0})^{(\mathrm{r})} f_{n_0}^{\alpha_0}(R_{\alpha_0}) \\ & - \frac{2\mu}{\hbar^2} \sum_n (\mathscr{T}_{\alpha' n' \alpha n} + \mathscr{V}_{\alpha' n' \alpha n}) \int_0^\infty \mathrm{d}R'_\alpha\, {}^{(\mathrm{i})}f_n^{\alpha}(R_\alpha^>)\, {}^{(\mathrm{r})}f_n^{\alpha}(R_\alpha^<) \zeta_{\alpha n}^{\alpha_0 n_0}(R'_\alpha).\end{aligned} \tag{18}$$

Then using the fact that

$$\left(\frac{\mathrm{d}^2}{\mathrm{d}R_{\alpha_0}^2} - V_{\alpha_0 n}^{\mathrm{D}}(R_\alpha) - \frac{l_{\alpha_0 n_0}(l_{\alpha_0 n_0}+1)}{R_{\alpha_0}^2} k_{\alpha_0 v_{n_0} j_{n_0}}^2\right)^{(\mathrm{r})} f_n^{\alpha_0}(R_\alpha) \equiv 0 \tag{19}$$

and eqn (11), we find

$$\begin{aligned}\zeta_{\alpha' n'}^{\alpha_0 n_0}(R_{\alpha'}) = {} & \mathscr{V}_{\alpha' n' \alpha_0 n_0}\, {}^{(\mathrm{r})}f_{n_0}^{\alpha_0}(R_{\alpha_0}) - \frac{2\mu}{\hbar^2} \sum_n \mathscr{D}_{\alpha' n' \alpha n} \zeta_{\alpha n}^{\alpha_0 n_0} \\ & - \frac{2\mu}{\hbar^2} \sum_n \mathscr{V}_{\alpha' n' \alpha n} \int_0^\infty \mathrm{d}R'_\alpha\, {}^{(\mathrm{i})}f_n^{\alpha}(R_\alpha^>)\, {}^{(\mathrm{r})}f_n^{\alpha}(R_\alpha^<) \zeta_{\alpha n}^{\alpha_0 n_0}(R'_\alpha)\end{aligned} \tag{20}$$

where the effect of $\mathscr{D}_{\alpha' n' \alpha n}$ acting on $\zeta_{\alpha n}^{\alpha_0 n_0}$ is defined as

$$\begin{aligned}\mathscr{D}_{\alpha' n' \alpha n} \zeta_{\alpha n}^{\alpha_0 n_0}(R_\alpha) = {} & \frac{\hbar^2}{2\mu}(1 - \delta_{\alpha\alpha'}) R_{\alpha'} \int \mathrm{d}\hat{R}_{\alpha'}\, \mathrm{d}\boldsymbol{r}_{\alpha'} \phi_{\alpha' n'}^*(\boldsymbol{r}_{\alpha'}, \hat{R}_{\alpha'}) [R_\alpha(\boldsymbol{R}_{\alpha'}, \boldsymbol{r}_{\alpha'})]^{-1} \\ & \times \phi_{\alpha n}[\boldsymbol{r}_\alpha(\boldsymbol{R}_{\alpha'}, \boldsymbol{r}_{\alpha'}), \hat{R}_\alpha(\boldsymbol{R}_{\alpha'}, \boldsymbol{r}_{\alpha'})] \zeta_{\alpha n}^{\alpha_0 n_0}[R_\alpha(\boldsymbol{R}_{\alpha'}, \boldsymbol{r}_{\alpha'})].\end{aligned} \tag{21}$$

Now the amplitude density $\zeta_{\alpha n}^{\alpha_0 n_0}$ is expanded in translational basis functions as

$$\zeta_{\alpha n}^{\alpha_0 n_0}(R_\alpha) = \sum_{m'} a_{\alpha n m'}^{\alpha_0 n_0} \lambda_{m'}^{\alpha n}(R_\alpha) \tag{22}$$

where the (real) basis functions $\lambda_m^{\alpha n}$ are not necessarily orthogonal. The overlap integrals of the translational basis functions are given by

$$\mathscr{O}_{m m'}^{\alpha n} = \int \mathrm{d}R_\alpha \lambda_m^{\alpha n}(R_\alpha) \lambda_{m'}^{\alpha n}(R_\alpha). \tag{23}$$

Substituting the expansion of eqn (22) into eqn (20), multiplying by $\lambda_m^{\alpha n}$ and integrating over $R_{\alpha'}$ gives

$$\sum_{m'} \mathscr{O}_{m m'}^{\alpha n} a_{\alpha n m'}^{\alpha_0 n_0} = b_{\alpha n m}^{\alpha_0 n_0} + \sum_{n' m'} C_{\alpha n m \alpha' n' m'} a_{\alpha' n' m'}^{\alpha_0 n_0} \tag{24}$$

where

$$b_{\alpha n m}^{\alpha_0 n_0} = \int \mathrm{d}R_\alpha\, \lambda_m^{\alpha n}(R_\alpha) \mathscr{V}_{\alpha n \alpha_0 n_0}\, {}^{(\mathrm{r})}f_{n_0}^{\alpha_0}(R_{\alpha_0}) \tag{25}$$

and

$$C_{\alpha n m \alpha' n' m'} = -\frac{2\mu}{\hbar^2}\int \mathrm{d}R_\alpha \lambda_m^{\alpha n}(R_\alpha)\Big(\mathscr{D}_{\alpha n \alpha' n'}\lambda_{m'}^{\alpha' n'}(R_{\alpha'}) + \mathscr{V}_{\alpha n \alpha' n'}\int_0^\infty \mathrm{d}R'_{\alpha'}\,{}^{(\mathrm{i})}f_{n'}^{\alpha'}(R_{\alpha'}^{>})\,{}^{(\mathrm{r})}f_{n'}^{\alpha'}(R_{\alpha'}^{<})\lambda_{m'}^{\alpha' n'}(R'_{\alpha'})\Big). \tag{26}$$

Thus, when $\zeta_{\alpha n}^{\alpha_0 n_0}$ is expanded in translational basis functions, $\mathscr{D}_{\alpha n \alpha n}\zeta_{\alpha n}^{\alpha_0 n_0}(R_\alpha)$ leads to overlap-type integrals.

In summary, comparing eqn (24) with eqn (18) we see that the kinetic-energy (derivative) operators occurring in the non-local operator $\mathscr{T}_{\alpha n \alpha' n'}$ vanish when acting on the inhomogeneity and yield simple overlap integrals when acting on the Green's function terms.

Eqn (24) can now be solved for the expansion coefficients $a_{\alpha n m}^{\alpha_0 n_0}$. In terms of these coefficients, eqn (17) for the coupling component of the reactance matrix is given by

$$\mathscr{K}_{n_\mathrm{f} n_\mathrm{i}} = -\frac{2\mu}{\hbar^2}\sum_m a_{\alpha_\mathrm{i} n_\mathrm{i} m}^{\alpha_\mathrm{i} n_\mathrm{i}}\int_0^\infty \mathrm{d}R_{\alpha_\mathrm{f}}\,{}^{(\mathrm{r})}f_{n_\mathrm{f}}^{\alpha_\mathrm{f}}(R_{\alpha_\mathrm{f}})\lambda_m^{\alpha_\mathrm{f} n_\mathrm{f}}(R_{\alpha\mathrm{f}}). \tag{27}$$

The full reactance matrix, with elements given by eqn (16), is related to the full scattering matrix and to state-to-state transition probabilities in the usual way.[18,19]

3. Application

As an illustration of the method just described, we present an application to the reaction $\mathrm{O}(^3P)+\mathrm{H}_2 \rightarrow \mathrm{OH}+\mathrm{H}$. In particular, we report total reaction probabilities with total angular momentum (J) equal to zero in the threshold regions for the $v=0$ and $v=1$ reactant vibrational levels. The potential-energy surface used in these calculations is a modified version[20] of the LEPS-type[21] surface of Johnson and Winter.[22]

The basis set used for the expansion is the outer product of an Arthurs-Dalgarno[23] rotational-orbital basis, an asymptotic vibrational eigenfunction basis expressed in terms of harmonic oscillator functions and a set of equally spaced Gaussians[24] distributed along the translational coordinate in each arrangement channel. The various basis-set and quadrature parameters for which we illustrate convergence are listed in table 1. The notation is as follows: $N_{\mathrm{rot}}(v)$ is the number of rotational states included in vibrational manifold v. The Gaussian basis overlap parameter c[24] appears in the sixth row. The next four rows list the location, $R_{1(G)}$, of the centre of the first Gaussian basis function, the distance $\Delta(G)$ between basis functions, the location $R_{N(G)}$ of the final Gaussian basis function, and the number $N(G)$ of the basis functions used to span this space. The next three rows list the finite-difference parameters used in solving for the distorted wave; $R_{1(\mathrm{F})}$ is the location of the first finite difference point, $\Delta(F)$ the spacing of the points, and $R_{N(\mathrm{F})}$ the final point. The distorted wave solutions are sometimes obtained on a finer grid than that on which the translational quadrature is performed, and the following two rows give the translational quadrature grid spacing $\Delta(R)$ and the total translational quadrature order N^{QR}. The next row lists N^{QA}, the order of the angular quadrature. The following four rows specify the vibrational quadrature. $N_{\alpha\alpha'}^{\mathrm{QV}}$ gives the total order of the extended trapezoidal rule used for the vibrational quadrature used in exchange matrix elements that are off-diagonal in arrangement channel. The values $r_<$ and $r_>$ are the minimum and maximum values of the vibrational coordinate included in the trapezoidal quadrature. The value $N_{\alpha\alpha}^{\mathrm{QV}}$ is the order of the modified Gauss-Hermite quadrature used for the $\mathscr{V}$ matrix elements diagonal in arrangement.

Table 2 presents some total distinguishable-atom reaction probabilities for $\mathrm{O}+\mathrm{H}_2(v,j=0) \rightarrow \mathrm{OH}+\mathrm{H}$ for initial reactant vibrational states $v=0$ and $v=1$ summed over the two identical final arrangement channels. The probabilities $>10^{-6}$ for the $v=0$

Table 1. Parameters for the calculations reported in table 2 for arrangement channels (α) $O+H_2$ and (β) $H+OH$

run:	1		2		3		4		5		6	
arrangement:	α	β	α	β	α	β	α	β	α	β	α	β
N_{rot} ($v=0$)	19	19	13	13	11	11	*a*	*b*	13	13	11	11
N_{rot} ($v=1$)	13	13	12	12	10	10	*a*	*b*	12	12	10	10
N_{rot} ($v=2$)	11	11	11	11	9	9	*a*	*b*	11	11	9	9
N_{rot} ($v=3$)	10	10	7	7	8	8	*a*	*b*	10	10	8	8
N_{rot} ($v=4$)	*c*	*c*	*c*	*c*	7	7	*c*	*c*	*c*	*c*	*c*	*c*
$C/a_0^{-1/2}$	1.4	1.4	*a*	*b*	*a*	*b*	1.2	1.2	1.4	1.4	*a*	*b*
$R_{1(G)}/a_0$	1.51	1.41	1.86	1.7	1.51	1.41	*a*	*b*	*a*	*b*	*a*	*b*
$\Delta(G)/a_0$	0.112	0.112	0.12	0.12	0.14	0.14	0.112	0.112	0.14	0.14	*a*	*b*
$R_{N(G)}/a_0$	7.95	5.89	7.38	7.22	7.95	5.89	7.21	5.89	7.95	5.89	*a*	*b*
$N(G)$	41	33	47	47	41	33	51	41	41	33	47	33
$R_{1(F)}/a_0$	0.8	0.8	1.5	1.3	0.8	0.8	*a*	*b*	*a*	*b*	*a*	*b*
$\Delta(F)/a_0$	0.01	0.01	0.005	0.01	0.01	0.01	0.008	0.008	0.01	0.01	*a*	*b*
$R_{N(F)}/a_0$	14.8	11.8	10.5	12.3	14.8	11.8	15.2	11.8	14.8	11.8	*a*	*b*
$\Delta(R)/a_0$	0.1	0.01	0.02	0.02	0.01	0.01	0.008	0.008	0.01	0.01	*a*	*b*
N^{QR}	50	50	29	29	50	50	*a*	*b*	*a*	*b*	*a*	*b*
N^{QA}	30	30	*a*	*b*	*a*	*b*	28	28	*a*	*b*	*a*	*b*
$N^{QV}_{\gamma\gamma'}$	34	34	39	39	34	34	34	38	34	34	*a*	*b*
$r_</a_0$	0.5	0.9	0.5	*b*	0.6	*b*	*a*	0.8	*a*	0.9	*a*	*b*
$r_>/a_0$	3.2	3.6	3.4	*b*	3.2	*b*	*a*	3.7	*a*	3.6	*a*	*b*
$N^{QV}_{\gamma\gamma}$	14	15	*a*	*b*	*a*	*b*	13	13	14	15	*a*	*b*

[a] Value is the same as in the α channel two columns to the left. [b] Value is the same as in the β channel two columns to the left. [c] $v=4$ level was not included in this run.

Table 2. Selected probabilities $P_{v=0,j=0}$; $P_{v=1,j=0}$ for $O+H_2(v,j) \rightarrow H+OH$ summed over identical arrangements at several total energies for the basis set and quadrature parameters listed in table 1

energy[a] /kcal mol^{-1}	1	2	3	4	5	6
10.0	*b*	2.8 (−8)[c]	2.4 (−8)	[b]	2.4 (−8)	2.4 (−8)
11.0	*b*	1.62 (−6)	1.61 (−6)	1.57 (−6)	1.61 (−6)	1.62 (−6)
12.0	*b*	3.75 (−5)	3.75 (−5)	3.76 (−5)	3.76 (−5)	3.77 (−5)
13.0	*b*	5.27 (−4)	5.12 (−4)	4.95 (−4)	5.12 (−4)	5.12 (−4)
14.0	*b*	4.64 (−3)	4.56 (−3)	4.48 (−3)	4.55 (−3)	4.54 (−3)
15.0	*b*	2.67 (−2)	2.59 (−2)	2.49 (−2)	2.57 (−2)	2.56 (−2)
16.0	*b*	8.46 (−2)	8.41 (−2)	8.20 (−2)	8.40 (−2)	8.37 (−2)
17.0	*b*	1.39 (−1)	1.37 (−1)	1.35 (−1)	1.37 (−1)	1.36 (−1)
18.0	*b*	1.64 (−1)	1.65 (−1)	1.63 (−1)	1.65 (−1)	1.64 (−1)
19.0	*b*	1.89 (−1); 9.46 (−8)	1.88 (−1); 9.06 (−8)	1.87 (−1); 8.76 (−8)	1.88 (−1); 8.82 (−8)	1.87 (−1); 8.40 (−8)
20.0	2.25 (−1); 8.86 (−6)[d]	2.25 (−1); 8.67 (−6)	2.25 (−1); 8.71 (−6)	2.21 (−1); 7.80 (−6)	2.25 (−1); 8.85 (−6)	2.24 (−1); 8.11 (−6)
21.0	2.63 (−1); 6.20 (−4)	2.62 (−1); 6.23 (−4)	2.63 (−1); 6.21 (−4)	2.61 (−1); 5.72 (−4)	2.63 (−1); 6.22 (−4)	2.62 (−1); 6.00 (−4)
22.0	2.80 (−1); 4.57 (−2)	2.81 (−1); 4.84 (−2)	2.80 (−1); 4.74 (−2)	2.80 (−1); 4.37 (−2)	2.80 (−1); 4.56 (−2)	2.80 (−1); 4.55 (−2)
23.0	3.10 (−1); 2.38 (−1)	3.10 (−1); 2.40 (−1)	3.10 (−1); 2.36 (−1)	3.07 (−1); 2.35 (−1)	3.10 (−1); 2.38 (−1)	*b*
24.0	*b*	3.36 (−1); 2.43 (−1)	3.30 (−1); 2.51 (−1)	3.34 (−1); 2.43 (−1)	3.38 (−1); 2.46 (−1)	*b*

[a] The zero of energy is the $O+H_2$ potential asymptote. [b] Not included. [c] This means $P_{00}=2.8\times10^{-8}$. [d] This means $P_{00}=2.25\times10^{-1}$ and $P_{10}=8.86\times10^{-6}$.

initial state appear to be converged to 4% or better with respect to small changes in the basis set and quadrature parameters. Runs numbered 2 and 4 show deviations of *ca.* 7% at the total energies of 13 and 15 kcal mol^{-1}, but we discount these because the radial quadrature order N^{QA} in run 4 is minimal for the width of the Gaussian basis used in that run. The probabilities $>10^{-5}$ for the $v=1$ initial state appear converged to *ca.* 10% or better (if, again, we discount run number 4, they appear to be converged to *ca.* 6% or better), and those probabilities $<10^{-5}$ appear to be converged to *ca.* 14%. The unitarity condition of the scattering matrix is well satisfied; all columns of the scattering matrix for the reported runs satisfy unitarity to better than 1% except for run number 3 at total energy 24 kcal mol^{-1}; the results for this run shows a maximum deviation of 1.5%.

4. Variational Transition-state Theory with Semiclassical Tunnelling

Approximate methods for calculating threshold energies and tunnelling probabilities for chemical reactions are of great interest for applications to larger (polyatomic) reactants. In the present case the accurate quantum-mechanical reaction probabilities provide a rare opportunity (previous work is summarized elsewhere[25]) to test these methods for realistic reactions in three dimensions. This includes probabilities for reaction from the first excited vibrational state as well as those for reaction from the ground vibrational state at energies near threshold. In the present article we test the predictions of quantized variational transition-state theory (VTST)[26-28] for selected-vibrational-state threshold energies and of the least-action (LA) semiclassical approximation[29] for tunnelling probabilities.

In quantized VTST, we begin by defining a reaction path, here taken as the minimum-energy path (MEP), and we compute quantized energy levels for the degrees of freedom orthogonal to this path. The threshold energies for classical reaction-coordinate motion for a system with a state-selected stretching vibration are given by the maxima of the state-selected vibrationally adiabatic potential curves defined by[26,27,30,31]

$$V_a^G(v, s) = V_{MEP}(s) + \varepsilon_{str}(v, s) + \varepsilon_{other}^G(s) \tag{28}$$

where s denotes the reaction coordinate (signed distance along the reaction path), $V_{MEP}(s)$ is the Born–Oppenheimer potential along the MEP, $\varepsilon_{str}(v, s)$ is the quantized eigenenergy of the vibrational mode that correlates adiabatically to the selected stretch, v is the vibrational quantum number of this stretch and $\varepsilon_{other}^G(s)$ is the ground-state, zero-angular-momentum zero-point energy of all the other bound modes. In the present case, since the MEP is collinear, $\varepsilon_{other}^G(s)$ is the zero-point of the doubly degenerate bending mode. [The adiabatic potential curve of eqn (28) is a familiar quantity, also appearing in statistical adiabatic models, the adiabatic theory of reactions and the statistical adiabatic channel model.[32-41] Brief reviews of other applications of adiabaticity to selected vibrational modes are given elsewhere.[30,42,43]] The potential curves $V_{MEP}(s)$, $V_a^G(v=0, s)$ and $V_a^G(v=1, s)$ defined by eqn (28) for the reactions examined here are presented in fig. 2.

The least-action tunnelling approximation is consistent with quantized VTST in that it assumes that the classical turning points for tunnelling are given by the locations at which the total energy E equals the vibrationally adiabatic potential curves of eqn (28). However, it also allows for tunnelling to occur prior to the system reaching this turning point. For systems with small reaction-path curvature the most successful semiclassical tunnelling approximations are based upon a reaction-path Hamiltonian in curvilinear coordinates including s and the coordinates orthogonal to it. In these coordinates the potential takes a simple expression, but the kinetic energy is complicated by the presence of terms proportional to the curvature of the reaction path. The semiclassical adiabatic methods which are most successful force the tunnelling to occur along specified paths

through the interaction region which 'cut the corner' to shorten the length of the tunnelling path.[44,45] In these methods the multidimensional scattering problem may be reduced[45] to the much simpler problem of tunnelling through a one-dimensional effective potential given by eqn (28) with an s-dependent effective mass. The curvilinear coordinates involved in these methods are not useful and the adiabatic approximation breaks down in regions along the reaction path which have large curvature. This type of behaviour occurs in systems in which the angle between the reaction path in the reactant and product channel (in mass-scaled coordinates) is small. For systems with small skew angles the tunnelling has been treated successfully by models which assume that tunnelling occurs along the most direct paths (straight lines) connecting the reactant and product regions.[46-48] In such models the tunnelling method is still based upon the reaction path Hamiltonian in those regions for which the reaction-path curvature is not too severe and the curvilinear coordinates are still useful. In classically allowed regions, the adiabatic approximation is used to define the caustics parallel to the reaction coordinates which define the termini of the tunnelling paths. Tunnelling is promoted by motion in the vibrational coordinate and, for a given total energy, can begin at many locations along a caustic in the asymptotic reactant region up to the turning point in the vibrationally adiabatic potential curve.

The least-action tunnelling method[29] unifies the large-curvature and small-curvature adiabatic tunnelling methods to provide a more general method which is applicable to reactions with small-to-large curvature of the reaction path and which is expected to be most accurate for systems such as $O+H_2$ which have intermediate curvature. In this method the optimum tunnelling path is chosen from a set of parametrized paths by requiring it to be the one that accumulates the least imaginary action along the tunnelling path. The least-action method is also capable of treating non-adiabatic tunnelling[48,49] in which the final vibrational state is not the same as the initial one. This is especially important for reactions which are very exoergic, allowing population of several final vibrational states, and for reactions from excited initial states which can proceed to the ground state of products. These vibrationally non-adiabatic processes become more important for reactions with regions of large reaction-path curvatures.

The reactions considered here are nearly thermoneutral and we treat all tunnelling of ground-state reagents as populating only the ground state of products. For the reactions $O+H_2(v=1) \rightarrow OH+H$ and $OH(v=1)+H \rightarrow O+H_2$ vibrational non-adiabaticity may be important because of the moderate reaction-path curvature, and for these excited-state reactions we use the partial-reaction-path (PRP) adiabaticity approximation,[50] which assumes that the reaction remains adiabatic until the region where the reaction-path curvature becomes appreciable and the probability of a non-adiabatic transition thus becomes likely. In applications, the reaction is assumed to remain strictly adiabatic up to a location s_+, where a sudden non-adiabatic transition occurs to the ground state. The location s_+ is chosen near the first occurrence of an appreciable local maximum of the reaction-path curvature. For the $O+H_2(v=1) \rightarrow OH+H$ and $OH(v=1)+H \rightarrow O+H_2$ reactions these locations occur after the first maximum in the adiabatic potential (which is different for the forward and reverse reactions), and for the present applications the location of the sudden transition is chosen at the local minimum of the state-selected $v=1$ adiabatic barrier on one side of the region of large reaction-path curvature and the OH + H reaction is controlled by a (smaller) O—H···H-like barrier on the other side.

Tunnelling probabilities for a total energy E and stretching vibrational state v as calculated by the least-action method are denoted $P^{LA}(E, v=0)$ or $P^{LAG}(E)$ for the ground state and $P^{LA}(E, v=1)$ for the excited states. Summing over all states of the bending modes for total angular momentum zero[51] gives the least-action approximation to the $J=0$ cumulative reaction probability $P_{cum}^{J=0}(E)$, to be compared with the quantum-mechanical $J=0$ cumulative reaction probability $P_{cum}^{J=0}(E)$, which is given by the sum

of all energetically allowed state-to-state reaction probabilities for a given initial vibrational level (*i.e.* summed over initial rotational quantum number and final rotational and vibrational quantum numbers). In the least-action calculations the contributions from excited states are approximated, analogous to the approximation used in the collinear exact quantum bend-corrected ground-state (CEQB/G) method,[51] from the least-action ground-state tunnelling probabilities, yielding

$$P^{\mathrm{LA}}_{\mathrm{cum}}(E, v) = P^{\mathrm{LA}}(E, v) + \sum_{i \neq 0} P^{\mathrm{LA}}\{E - \varepsilon_{\mathrm{int}}[v, i, s = s^{\mathrm{A}}_{*}(v)] + \varepsilon_{\mathrm{int}}[v, i, s^{\mathrm{A}}_{*}(v)], v\} \quad (29)$$

where $s^{\mathrm{A}}_{*}(v)$ is the location of the maximum of eqn (28), the sum is over excited $J = 0$ bend states (thus $i = 0$ corresponds in the usual notation[52] to 0^0, $i = 1$ to 2^0, $i = 2$ to 4^0 *etc.*) and $\varepsilon_{\mathrm{int}}$ is the energy of the bound modes orthogonal to s.

The calculational details are as described elsewhere.[27,29,53] Energy levels for the stretching vibrations are calculated using the actual stretching potential by the WKB approximation.[53] Energy levels for the bending vibrations are calculated using a harmonic-quartic approximation to the bending potential with Taylor-series force constants.[27] The energy levels of the harmonic-quartic potential are obtained using a perturbation-variation method.[54]

For $O + H_2$ (but not $OH + H$) the results calculated by eqn (29) are multiplied by two because we consider the sum over the two possible $OH + H$ product arrangements ($OH + H'$ and $OH' + H$).

5. Comparisons and Discussion

The cumulative probabilities for the reaction $O + H_2(v) \rightarrow OH + H$ for $v = 0$ and $v = 1$ are shown in fig. 1. (The zero of energy for all figures is the $O + H_2$ potential asymptote.) The solid curves are the semiclassical results of eqn (29), including the factor of two, and the symbols are the quantum-mechanical results summed over all states of $OH + H'$ and $OH' + H$. The left-hand curve represents the results for initial vibrational quantum number $v = 0$ in the threshold region and the right-hand curve those for $v = 1$ over the cumulative probability range of 10^{-7} to 10^{-1}. The accurate and semiclassical methods agree very well for $v = 0$ and reasonably well for $v = 1$. (The wavering about a smooth curve of the semiclassical probabilities above 10^{-1} for $v = 0$ appears to result from the classical turning points being located in a region of high reaction-path curvature.)

The classical barrier height for the surface[20,22] employed here is 12.5 kcal mol^{-1}, at which energy the cumulative probability is *ca.* 10^{-3}. Therefore, the energy range shown includes energies quite far above the saddle point energy as well as those deep into the tunnelling region. It is encouraging that the semiclassical method works so well in both energy regions. The accurate results in fig. 1 can also be used to test the distorted wave approximation,[20,25,55] and this is done elsewhere.[9]

The energy of the $H_2(v = 1, j = 0)$ state is 18.0 kcal mol^{-1}. As can be seen from fig. 1, the $v = 1$ reaction 'turns on' at *ca.* 19 kcal mol^{-1} of total energy, corresponding to an initial relative translational energy of *ca.* 1 kcal mol^{-1}, showing clearly that the vibrational excitation energy is not entirely available for reaction. The semiquantitative correspondence of the accurate and semiclassical $v = 1$ results in fig. 2 means that the adiabatic approximation employed in the latter are apparently valid in this case, and they do provide a simple estimate of how much of the vibrational energy is available for reaction. To obtain a more quantitative measure of the validity of the adiabatic approximation we compare VTST and accurate threshold energies in table 3.

Table 3 shows two VTST threshold energies for the $v = 1$ reactions. The first is the highest adiabatic potential encountered by the system prior to the region of high reaction-path curvature; this is labelled PRP (partial reaction path). The second is the highest adiabatic potential encountered at any point along the reaction path; this is

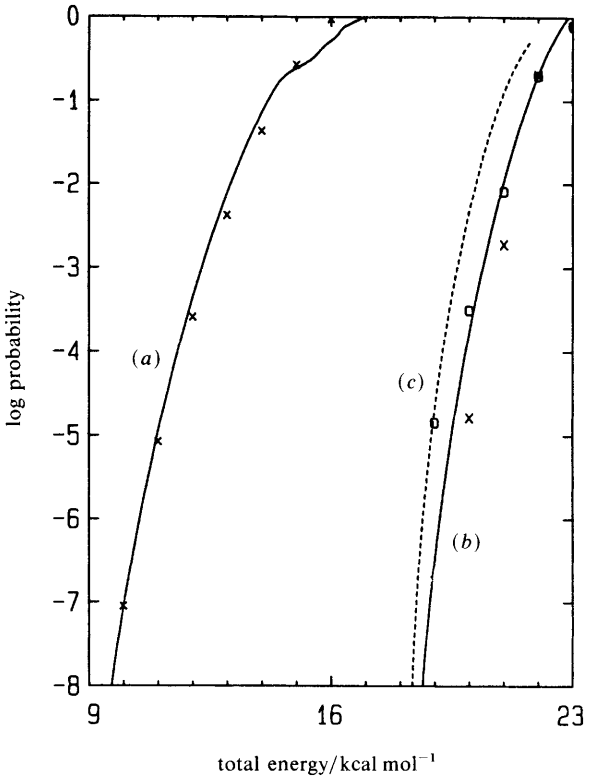

Fig. 1. Logarithm of the cumulative reaction probability vs. total energy. The solid curves are the approximate cumulative reaction probabilities from eqn (29) for the forward reaction $O + H_2(v) \rightarrow OH + H$ for $v = 0$ (*a*) and $v = 1$ (*b*). Crosses denote the accurate cumulative reaction probability for this reaction for $v = 0$ and $v = 1$. (*c*) The dashed curve is the approximate cumulative reaction probability from eqn (29) for the reverse reaction $H + HO(v = 1) \rightarrow O + H_2$. Circles denote the accurate cumulative reaction probability for this reaction. The cross and circle at 22 kcal mol^{-1} are accidently coincident, and the cross for 23 kcal mol^{-1} is off scale.

labelled FRP (full reaction path). There is even more uncertainty regarding the value to list as the threshold for the quantal studies. For all the quantal thresholds in table 3, we list the range of (interpolated) total energy at which the $j = 0$ reaction probability, summed over all final states, is a factor of 0.4 to 0.5 of that at a total energy of 24 kcal mol^{-1}, which is the highest energy for which we have made accurate calculations. The reaction probabilities for $O + H_2(v, j = 0)$ and $H + HO(v, j = 0)$ for $v = 0$ and 1 are shown in fig. 3. Comparison of the threshold energies listed in table 3 with fig. 3 shows that our definition of the threshold energy corresponds to the region in which the reaction probability is flattening out. The VTST and quantal thresholds for $O + H_2(v = 1)$ agree within 0.5–0.7 kcal mol^{-1}.

The cumulative probabilities for the reverse reaction, $OH(v = 1) + H \rightarrow O + H_2$, are also shown in fig. 1. (The $v = 0$ probabilities for the forward and backward reaction differ from each other only by an arrangement channel multiplicity factor of two, so the $v = 0$ reverse reaction does not provide an independent test and is not included.) For the $v = 1$ case the accurate and semiclassical probabilities for the reverse reaction differ by *ca.* one order of magnitude for total energies above *ca.* 20 kcal mol^{-1} with the semiclassical method overestimating the reaction probability. Since the quantum results for this case appear to be converged with respect to numerical parameters to the same

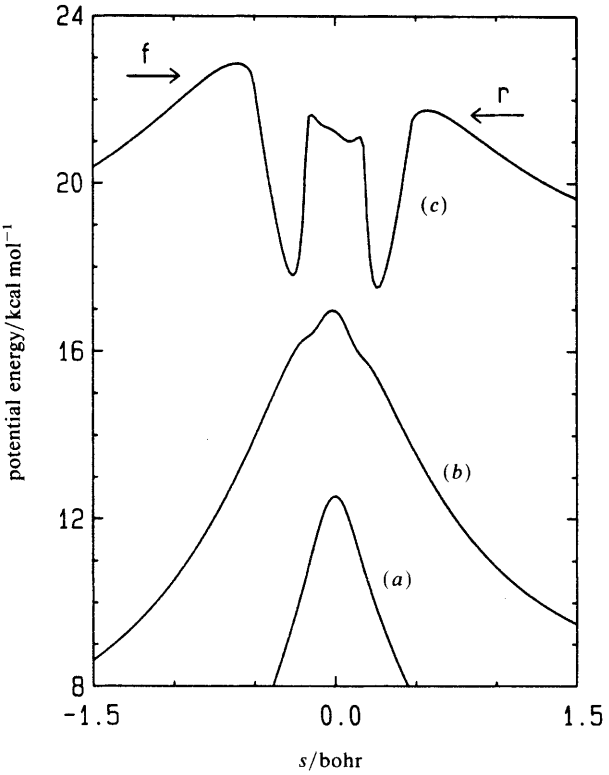

Fig. 2. Values of the Born-Oppenheimer potential energy V_{MEP} (a) and vibrationally adiabatic potential curves for $v=0$ (b) and $v=1$ (c) defined by eqn (28) *vs.* reaction coordinate s. The directions of the forward (f) and reverse (r) reactions are indicated by arrows.

Table 3. Threshold energies

reaction	total energy threshold/kcal mol^{-1}		
	VTST-PRP	VTST-FRP	quantal
$O+H_2(v=0)$	—	17.0	16.8-17.6
$O+H_2(v=1)$	22.9	22.9	22.2-22.4
$H+OH(v=0)$	—	17.0	16.3-17.0
$H+OH(v=1)$	21.6	22.9	22.0-22.3

extent as for the $O+H_2$ reaction discussed in section 3, one interpretation of the difference of the two sets of $v=1$ probabilities in fig. 1 is that the reverse $v=1$ reaction is even more vibrationally adiabatic than is assumed in the semiclassical method. The disagreement between the methods can be interpreted as involving the location of $s_+(v=1)$, where the sudden non-adiabatic transition occurs, as discussed in section 4. If the reaction were assumed not to become appreciably non-adiabatic prior to reaching the O···H—H-like adiabatic maximum, which is higher than the O—H···H-like maximum (see fig. 2), the VTST-plus-semiclassical-tunnelling results would all be smaller. Table 3 shows that the first VTST adiabatic maximum for $OH(v=1)+H$ is 1.3 kcal mol^{-1} lower than the fully adiabatic maximum and the $P^{LA}_{cum}(v=1)$ curve for the reverse reaction is accordingly shifted to the left in fig. 1 (the shift is less than 1.3 kcal mol^{-1} because

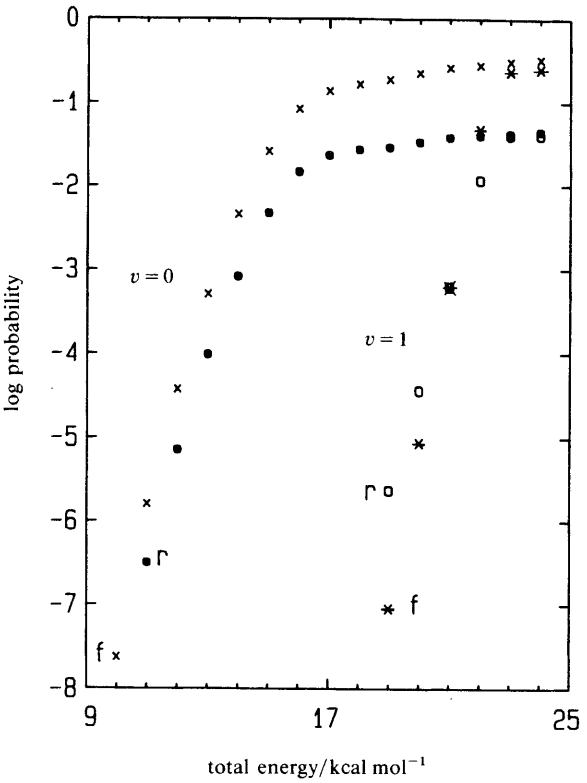

Fig. 3. Logarithm of the accurate reaction probability *vs.* total energy for the forward (f) reaction $O+H_2(v=0, j=0) \rightarrow OH+H$ (×) and $O+H_2(v=1, j=0) \rightarrow OH+H$ (*) and for the reverse (r) reaction $H+HO(v=0, j=0) \rightarrow O+H_2$ (●) and $H+HO(v=1, j=0) \rightarrow O+H_2$ (○).

the forward curve involves a factor-of-2 arrangement degeneracy factor). However, the accurate quantal results in fig. 1 and 3 and the quantal threshold energy given in table 3 show a much smaller shift, indicating that the higher adiabatic barrier controls the reaction in both directions. Thus the accurate quantal threshold is intermediate between the PRP and FRP predictions, which is similar to what was found for this reaction in the collinear world in ref. (50).

The remaining rearrangement reaction for the system studied here is the exchange reaction $H+OH' \rightarrow H'O+H$. On the surface used here,[20] the classical barrier height for this process is 35.7 kcal mol^{-1} above the OH + H potential asymptote, corresponding to a total energy of 38.5 kcal mol^{-1} for the zero of energy used here (see footnote *a* of table 2). At the energies we have been examining the reaction probabilities for the exchange reaction are 4 to 10 orders of magnitude smaller than those for the $O+H_2$ reaction and its reverse.

6. Conclusions

The good convergence of the present accurate quantal-dynamical calculations is very encouraging, especially since the method has some particularly attractive computational aspects. First, it is very well suited to currently available large-memory vector computers. Secondly, it allows for several possible stages of refinement, including more rapidly convergent translational bases, multichannel distortion potentials, and the use of a variational functional.[10] (Even without these refinements the method has already been

applied to the reaction $HBr + H \rightarrow H_2 + Br$.[56] which is more exothermic, and hence more difficult to converge, than either the forward or reverse reaction studied here.)

The comparisons of VTST threshold energies and least-action semiclassical tunnelling probabilities to the present accurate dynamical results show excellent agreement for the ground vibrational state and for the $O + H_2(v = 1)$ reaction; this confirms the expected utility of these methods based on previous tests for $H + H_2(v = 1)$[57] and $D + H_2(v = 1)$.[5] For $OH(v = 1) + H$ the comparison of approximate and accurate reaction probabilities again indicates that the vibrationally adiabatic barriers do limit the reactive flux, but quantitative approximate calculations are less certain because the highest vibrationally adiabatic barrier occurs on the product side of the region of highest reaction-path curvature.

This work was supported in part by the National Science Foundation and the Minnesota Supercomputer Institute. In addition, work at Chemical Dynamics Corp. was supported by the U.S. Army Research Office under contract DAAG-29-84-C-0011.

References

1 *The Theory of Chemical Reaction Dynamics*, ed. D. C. Clary (D. Riedel, Dordrecht, 1986).
2 D. W. Schwenke and D. G. Truhlar, in *Supercomputer Simulations in Chemistry*, ed. M. Dupuis (Springer-Verlag, Berlin, 1986), p. 165.
3 L. Castillego, I. C. Percival and M. J. Seaton, *Proc. R. Soc. London, Ser. A*, 1960, **254**, 259.
4 D. W. Schwenke, D. G. Truhlar and D. J. Kouri, *J. Chem. Phys.*, 1987, **86**, 2772.
5 K. Haug, D. W. Schwenke, Y. Shima, D. G. Truhlar, J. Zhang and D. J. Kouri, *J. Phys. Chem.*, 1986, **90**, 6757.
6 J. Zhang, D. J. Kouri, K. Haug, D. W. Schwenke, Y. Shima and D. G. Truhlar, *J. Chem. Phys.*, submitted.
7 Z. C. Kuruoglu and F. S. Levin, *Phys. Rev. Lett.*, 1982, **48**, 899.
8 Z. C. Kuruoglu and F. S. Levin, *Ann. Phys.*, 1985, **163**, 149.
9 K. Haug, D. W. Schwenke, D. G. Truhlar, Y. Zhang, J. Z. H. Zhang and D. J. Kouri, *J. Chem. Phys.*, submitted.
10 D. W. Schwenke, K. Haug, M. Zhao, D. G. Truhlar, Y. Sun, J. Zhang and D. J. Kouri, to be published.
11 P. G. Burke and K. Smith, *Rev. Mod. Phys.*, 1962, **34**, 458.
12 D. G. Truhlar, in *Semiempirical Methods of Electronic Structure Calculation, Part B*, ed. G. Segal (Plenum, Press, New York, 1977), p. 247.
13 W. H. Miller, *J. Chem. Phys.*, 1969, **50**, 407.
14 D. G. Truhlar, J. Abdallah Jr, and R. L. Smith, *Adv. Chem. Phys.*, 1974, **25**, 211.
15 M. K. Gailitis, in *Effective Cross Sections for the Collision of Electrons with Atoms: Atomic Collisions III*, ed. V. I. Veldre (Latvian Academy of Sciences, Riga, 1965).
16 P. G. Burke and A. J. Taylor, *Proc. Phys. Soc. London*, 1966, **88**, 549.
17 R. K. Nesbet, *Adv. At. Mol. Phys.*, 1977, **13**, 315.
18 J. M. Blatt and L. C. Biedenharn, *Rev. Mod. Phys.*, 1952, **24**, 258.
19 M. A. Brandt, D. G. Truhlar and R. L. Smith, *Comput. Phys. Commun.*, 1973, **5**, 456; 1974, **7**, 177(E).
20 G. C. Schatz, *J. Chem. Phys.*, 1985, **83**, 5677.
21 S. Sato, *J. Chem. Phys.*, 1955, **23**, 592.
22 B. R. Johnson and N. W. Winter, *J. Chem. Phys.*, 1977, **66**, 4116.
23 A. M. Arthurs and A. Dalgarno, *Proc. R. Soc. London, Ser. A*, 1960, **256**, 540.
24 I. P. Hamilton and J. C. Light, *J. Chem. Phys.*, 1986, **84**, 306.
25 B. C. Garrett, D. G. Truhlar and G. C. Schatz, *J. Am. Chem. Soc.*, 1986, **108**, 2876.
26 B. C. Garrett and D. G. Truhlar, *J. Phys. Chem.*, 1979, **83**, 1079; errata: 1980, **84**, 682; 1983, **87**, 4553.
27 B. C. Garrett, D. G. Truhlar, R. S. Grev and A. W. Magnuson, *J. Phys. Chem.*, 1980, **84**, 1730; erratum: 1983, **87**, 4554.
28 D. G. Truhlar and B. C. Garrett, *Acc. Chem. Res.*, 1980, **13**, 440.
29 B. C. Garrett and D. G. Truhlar, *J. Chem. Phys.*, 1983, **79**, 4931.
30 D. G. Truhlar and A. D. Isaacson, *J. Chem. Phys.*, 1982, **77**, 3516.
31 R. Steckler, D. G. Truhlar and B. C. Garrett, *J. Chem. Phys.*, 1986, **84**, 6712.
32 R. A. Marcus, *J. Chem. Phys.*, 1965, **43**, 1598.
33 R. A. Marcus, *J. Chem. Phys.*, 1966, **45**, 2630.
34 R. A. Marcus, *J. Chem. Phys.*, 1966, **45**, 4493.
35 M. S. Child, *Proc. R. Soc. London, Ser. A*, 1966, **292**, 272.
36 R. A. Marcus, *J. Chem. Phys.*, 1967, **46**, 959.

37 R. A. Marcus, *Discuss. Faraday Soc.*, 1968, **44**, 7.
38 M. S. Child, *Discuss. Faraday Soc.*, 1968, **44**, 68.
39 R. A. Marcus, *J. Chem. Phys.*, 1969, **49**, 2617.
40 D. G. Truhlar, *J. Chem. Phys.*, 1970, **53**, 2041.
41 M. Quack and J. Troe, *Ber. Bunsenges. Phys. Chem.*, 1974, **78**, 240.
42 D. G. Truhlar and R. E. Wyatt, *Annu. Rev. Phys. Chem.*, 1976, **27**, 1.
43 D. G. Truhlar and B. C. Garrett, *Annu. Rev. Phys. Chem.*, 1984, **35**, 159.
44 R. A. Marcus and M. E. Coltrin, *J. Chem. Phys.*, 1977, **67**, 2609.
45 R. T. Skodje, D. G. Truhlar and B. C. Garrett, *J. Chem. Phys.*, 1982, **77**, 5955.
46 B. C. Garrett, D. G. Truhlar, A. F. Wagner and T. H. Dunning Jr, *J. Chem. Phys.*, 1983, **78**, 4400.
47 D. K. Bondi, J. N. L. Connor, B. C. Garrett and D. G. Truhlar, *J. Chem. Phys.*, 1983, **78**, 5981.
48 B. C. Garrett, N. Abusalbi, D. J. Kouri and D. G. Truhlar, *J. Chem. Phys.*, 1985, **83**, 2252.
49 M. M. Kreevoy, D. Ostovic, D. G. Truhlar and B. C. Garrett, *J. Phys. Chem.*, 1986, **90**, 3766.
50 B. C. Garrett, D. G. Truhlar, J. M. Bowman and A. F. Wagner, *J. Phys. Chem.*, 1986, **90**, 4305.
51 J. M. Bowman, *Adv. Chem. Phys.*, 1985, **61**, 115.
52 G. Herzberg, *Molecular Spectra and Molecular Structure. II. Infrared and Raman Spectra of Polyatomic Molecules* (D. Van Nostrand, Princeton, 1945), p. 217.
53 B. C. Garrett and D. G. Truhlar, *J. Chem. Phys.*, 1984, **81**, 309.
54 D. G. Truhlar, *J. Mol. Spectrosc.*, 1971, **38**, 415.
55 G. C. Schatz, *J. Chem. Phys.*, 1985, **83**, 5677.
56 Y. Zhang, J. Z. H. Zhang, D. J. Kouri, K. Haug, D. W. Schwenke and D. G. Truhlar, to be published.
57 B. C. Garrett and D. G. Truhlar, *J. Phys. Chem.*, 1985, **89**, 2204.

Received 18*th May*, 1987